Analyst

PAPER

View Article Online
View Journal | View Issue

Check for updates

Cite this: *Analyst*, 2019, **144**, 6914

Single droplet detection of immune checkpoints on a multiplexed electrohydrodynamic biosensor†

Alain Wuethrich, *[a] Aswin Raj Rajkumar, [c] Karthik Balaji Shanmugasundaram, [a] Kamil K. Reza, [a] Shuvashis Dey, [a] Christopher B. Howard, [a] Abu Ali Ibn Sina *[a,b] and Matt Trau *[a,c]

Monitoring soluble immune checkpoints in circulating fluids has the potential for minimally-invasive diagnostics and personalised therapy in precision medicine. Yet, the sensitive detection of multiple immune checkpoints from small volumes of liquid biopsy samples is challenging. In this study, we develop a multiplexed immune checkpoint biosensor (MICB) for parallel detection of soluble immune checkpoints PD-1, PD-L1, and LAG-3. MICB integrates a microfluidic sandwich immunoassay using engineered single chain variable fragments and alternating current electrohydrodynamic *in situ* nanofluidic mixing for promoting biosensor–target interaction and reducing non-specific non-target binding. MICB provides advantages of simultaneous analysis of up to 28 samples in <2 h, requires as little as a single sample drop (*i.e.*, 20 μL) per target immune checkpoint, and applies high-affinity yeast cell-derived single chain variable fragments as a cost-effective alternative to monoclonal antibodies. We investigate the assay performance of MICB and demonstrate its capability for accurate immune checkpoint detection in simulated patient serum samples at clinically-relevant levels. MICB provides a dynamic range of 5 to 200 pg mL^{-1} for PD-1 and PD-L1, and 50 to 1000 pg mL^{-1} for LAG-3 with a coefficient of variation <13.8%. Sensitive immune checkpoint detection was achieved with limits of detection values of 5 pg mL^{-1} for PD-1, 5 pg mL^{-1} for PD-L1, and 50 pg mL^{-1} for LAG-3. The multiplexing capability, sensitivity, and relative assay simplicity of MICB make it capable of serving as a bioanalytical tool for immune checkpoint therapy monitoring.

Received 31st July 2019,
Accepted 15th October 2019

DOI: 10.1039/c9an01450k

rsc.li/analyst

Published on 16 October 2019. Downloaded by University of Zurich on 1/3/2020 12:37:16 PM.

1. Introduction

Key to a functional immune system is the ability to induce a controlled immune response upon recognition of pathogens such as tumour cells. To evade the immune response, tumour cells can develop immune tolerance by displaying immune checkpoint molecules.[1] To revert this process, the targeted inhibition of immune checkpoints has emerged as a promising treatment strategy in precision medicine. For instance, the FDA approved inhibitory drugs are used to target PD-1 (programmed cell death protein 1) and PD-L1 (programmed death-ligand 1) in the treatment of multiple cancers.[2] LAG-3 (lymphocyte activation gene-3) is a relatively new drug target in clinical development and preliminary results strongly support its efficacy and safety profile in monotherapy and combined therapy with PD-1 for ovarian cancer, head and neck squamous cell carcinoma, and non-small cell lung cancer.[3] In addition to the therapeutic inhibition, the analysis of immune checkpoints serves as a promising therapy monitoring tool, where the measured changes in the immune checkpoint expression could support the clinician in targeted therapy selection. Potential synergistic effects have been found for PD-1, PD-L1, and LAG-3, which has also emphasised the need for multiplexed immune checkpoint analysis.[4,5]

Conventional analysis of immune checkpoints is performed by immunohistochemistry and genotyping of surgically removed tissue samples. Tissue sampling has limitations as it only reflects a relatively small area at a single time point which can result in misrepresentation of the tumour microenvironment and is further inapplicable for frequent therapy monitoring. As a minimally-invasive strategy for immune checkpoint analysis, liquid biopsy emerged as a readily accessible potential alternative to tissue biopsy.[6–8] To detect soluble immune checkpoints in liquid biopsies, common immunosorbent assay methods use relatively costly monoclonal and polyclonal antibodies for capturing and labeling targets

[a]*Centre for Personalized Nanomedicine, Australian Institute for Bioengineering and Nanotechnology (AIBN), The University of Queensland, Brisbane, QLD 4072, Australia. E-mail: a.wuethrich@uq.edu.au, a.sina@uq.edu.au, m.trau@uq.edu.au*
[b]*Department of Biochemistry & Molecular Biology, Shahjalal University of Science & Technology, Bangladesh*
[c]*School of Chemistry and Molecular Biosciences, The University of Queensland, Brisbane, QLD4072, Australia*

†Electronic supplementary information (ESI) available. See DOI: 10.1039/c9an01450k

This journal is © The Royal Society of Chemistry 2019

Published on 16 October 2019. Downloaded by University of Zurich on 1/3/2020 12:37:16 PM.

prior to enzymatic, fluorescence, and colorimetric read-outs. Moreover, the limited shelf life and temperature stability of antibodies are common issues that affect antibody specificity, and ultimately the assay performance. Single-chain variable fragments (ScFvs) obtained from fragmented yeast cell membranes have emerged as alternative immunoaffinity reagents providing long shelf-life (*e.g.*, target specificity not compromised after storage at room temperature for up to one year) and can be mass-produced at relatively low costs.[9] We have previously explored these engineered nanoyeast ScFvs for various specific biosensing approaches and shown that nanoyeast ScFvs can be a viable alternative to monoclonal and polyclonal antibodies.[10,11]

Microfluidic biosensors provide an attractive option for simultaneous and sensitive detection of biomarkers including circulating tumour cells, circulating free DNA, proteins, and extracellular vesicles from liquid biopsies.[12–15] The small features of microfluidic devices with purpose-built structures enable the integration of a whole sample-to-answer procedure at minimal sample requirements and provide fast assay times.[16–19] These capabilities strongly support the development of immune checkpoint platforms for simple and sensitive detection of multiple targets with potential for clinical therapy monitoring. We have previously developed a unidirectional flow chip that applied alternating current electrohydrodynamics (ac-EHD) for sensitive and specific detection of soluble immune checkpoints.[10] A relatively large sample volume was passed through the chip and immune checkpoint detection was performed by surface-enhanced Raman spectroscopy which restricted the chip's clinical operation.

In this study, we develop a multiplexed immune checkpoint biosensor (MICB) for the analysis of soluble PD-1, PD-L1, and LAG-3 from liquid biopsies. To enable multiplexed detection from small sample volumes, MICB was designed to accommodate a single sample droplet (20 μL) on each of the 28 individual circular electrodes. ac-EHD nanofluidic mixing is induced within the sample droplet by the application of an electric field on the circular electrodes. The nanofluidic mixing stimulates immune checkpoint interaction with the nanoyeast ScFv-functionalised electrodes and reduces non-target sensor binding, thereby supporting specific immune checkpoint capture. MICB applies a simple and sensitive colorimetric read-out using the enzymatic conversion of 3,3′,5,5′-tetramethylbenzidine (TMB, colourless) to TMB oxidised (blue). We optimise the sensitivity of MICB and assess the analytical performance of the platforms. Finally, the potential of MICB for immune checkpoint monitoring in liquid biopsies was evaluated on simulated plasma samples where the present biosensor achieved clinically-relevant sensitivity.

2. Materials and methods

2.1 Preparation of nanoyeast ScFvs

The nanoyeast ScFvs for PD-1, PD-L1, and LAG-3 were produced from whole yeast according to the panning and fragmentation processes described by Li and co-workers.[20] A c-myc tag was cloned to the C-termini of the nanoyeast ScFvs. Successful expression of ScFvs on the yeast cells was confirmed by western blot analysis (ESI Fig. S1†).

2.2 Device fabrication

MICB was prepared similar to a previous report.[21] The device design and microfabrication process are shown in ESI Fig. S2 and S3,† respectively. Briefly, the electrode pattern including the connecting wire structure was designed using Layout Editor L-Edit V15 (Tanner Research, Monrovia, USA) and written on 5 inch soda lime chrome masks (Shenzhen Qingyi Precision Mask Making, Shenzhen, Singapore) using a direct write system μPG 101 (Heidelberg Instruments, Heidelberg, Austria). Next, a negative photoresist AZnLOF 2020 (Microchemicals GmbH, Ulm, Germany) was spin-coated for 30 s at 3000 rpm on a clean 4 inch boroflat wafer (Bonda Technology Pte Ltd, Down Town Core, Singapore). After a soft-bake (2 min, 110 °C), the wafer was UV-exposed with the above prepared mask at a constant dose of 200 mJ cm^{-1} using a mask aligner (EVG 620, EV Group, St Florian am Inn, Austria) following a post-exposure bake for 1 min at 110 °C, and subsequent wafer development for 45 s using a AZ726 MIF Developer (Microchemicals GmbH, Ulm, Germany). The gold electrodes were then created by deposition of 10 nm Ti and 200 nm gold using a Temescal FC-2000 Deposition System (Ferrotec, Livermore, USA) and overnight lift-off in Remover PG (Microchemicals GmbH, Ulm, Germany). The wafer carrying the gold electrode structures was rinsed with isopropanol and dried under a flow of nitrogen. To accommodate a single sample droplet, a polydimethylsiloxane (PDMS) well structure was prepared by curing activated silicon elastomer solution (Sylgard® 184, Dow, Midland, USA) for 20 min at 80 °C. Wells of 5 mm diameter were then punched into the PDMS slab and aligned with the electrode structures of the device. Device microfabrication was completed by thermal bonding of PDMS structures on the device for 2 h at 65 °C.

2.3 Device functionalisation

The nanoyeast ScFvs for PD-1, PD-L1, and LAG-3 were conjugated to the gold electrodes using biotin–avidin chemistry. First, a solution of 200 μg mL^{-1} biotinylated bovine serum albumin (Thermo Fisher Scientific, Scoresby, Australia) in phosphate buffered saline (PBS, 10 mM, pH 7.4) was incubated for 2 h at room temperature. Subsequently, incubations followed for 1 h using 100 μg mL^{-1} streptavidin (Thermo Fisher Scientific, Scoresby, Australia) in PBS, and 10 μg mL^{-1} biotinylated anti-hemagglutinin (ab26228, Abcam, Cambridge, UK) in PBS. Next, the target nanoyeast-ScFv solution (protein concentration approx. 300 μg ml^{-1}) was conjugated to the anti-hemagglutinin antibody functionalised electrode surface for 1 h at room temperature. Finally, device functionalisation was completed by a 1 h blocking step with 1% bovine serum albumin in PBS (Thermo Fisher Scientific, Scoresby, Australia). In between the conjugation steps, the electrodes were washed three times with PBS to remove the unbound bioreagents.

Published on 16 October 2019. Downloaded by University of Zurich on 1/3/2020 12:37:16 PM.

2.4 Immune checkpoint detection

All experiments were performed in accordance with the Helsinki Declaration and approved by the University of Queensland Human Research Ethics Committee (approval number: 2011001315). Informed consent was obtained from human participants of this study.

MICB was connected to a signal generator 33510B (Agilent Technologies, Mulgrave, Australia). The sample containing individual immune checkpoint standards or their mixture thereof was pipetted to the chip wells. Human serum samples were sourced from the Ventyx Wesley Research Institute Tissue Bank (Auchenflower, Australia) and used after 5-fold dilution with PBS. The recombinant human immune checkpoint standards PD-1, PD-L1, and LAG-3 were obtained from R&D Systems (Minneapolis, USA). After sample addition, an alternating current electric field of 500 Hz and 800 mV for 40 min was applied to induce ac-EHD nanoscopic mixing. Next, 20 μL of 2 μg mL^{-1} horseradish peroxidase (HRP)-conjugated secondary antibody in PBS was added to the well and incubated for 1 h to complete the assay complex. The HRP-conjugated secondary antibodies were anti-PD-1 (BP104328, clone 4F12), anti-PD-L1 (BP212046, clone MM012-9E5), and anti-LAG-3 (BP211764, clone MM0444-3C39) purchased from Novus Biologicals (Centennial, USA). HRP conjugation of these secondary antibodies was performed using the Lightning-Link HRP Antibody labelling kit (Novus Biologicals, Centennial, USA) and according to the manufacturer's protocol. In between the incubation steps, the device biosensors were washed three times with PBS. Finally, 20 μL of TMB solution (Thermo Fisher Scientific, Scoresby, Australia) was incubated for 20 min, the solution was transferred to a vial, and then the enzymatic reaction was quenched by adding 1 μL 2 M sulfuric acid prior to reading the absorbance measurement at 450 nm using a Nanodrop ND-1000 spectrophotometer (Thermo Fisher Scientific, Scoresby, Australia). All the incubation steps mentioned above were performed at room temperature.

3. Results and discussion

3.1 Principle of a multiplexed immune checkpoint biosensor (MICB)

To enable specific detection of immune checkpoints, we designed a MICB consisting of an array electrode; each electrode made of an inner circle and outer ring structure. MICB accommodates 28 electrodes embedded in PDMS wells that facilitate the simultaneous analysis of 28 samples (Fig. 1). We used our previously optimised electrode geometry which showed improved assay performance for the detection of different biomarkers.[21,22] Recent advances in microfabricated devices have significantly contributed to enabling highly sensitive and particularly high throughput analysis.[23–25] However, one of the major drawbacks of the current microfabricated devices is the slow mass transport of the analytes towards the sensor surface, which results in slow response time and nonspecific interference from the nontarget molecules. Our device used an alternating current electrohydrodynamic (ac-EHD) system developed in our lab that generates a nanoscopic fluid flow at the sensor surface. This nanomixing at the sensor surface significantly increases the mass transport of the target molecules and reduces the nonspecific interference.

Here we investigate the capabilities of nanofluidic mixing for multiplexed immune checkpoint detection in minute volumes of samples from liquid biopsies. Individual bio-

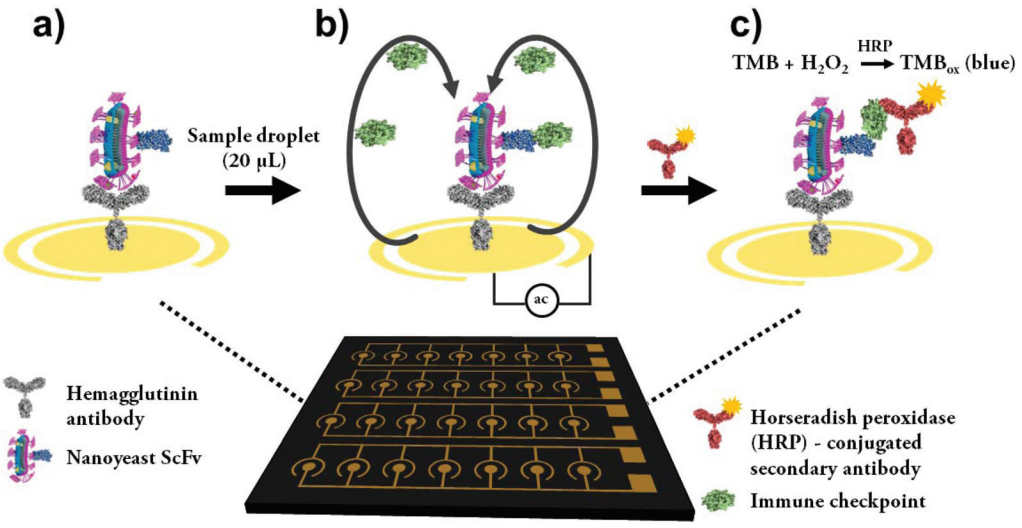

Fig. 1 Schematic of a multiplexed immune checkpoint biosensor (MICB). (a) To enable specific detection of soluble PD-1, PD-L1, and LAG-3, the electrodes are separately functionalised with target-specific nanoyeast ScFvs *via* specific conjugation using hemagglutinin tag/anti-hemagglutinin interaction. (b) A single sample droplet (20 μL) is added to each target on MICB followed by ac-EHD-induced nanoscopic mixing. (c) Incubation with the secondary antibody HRP-conjugate completes the immune complex. The addition of TMB solution causes a colour change where the solution's absorbance value is proportional to the immune checkpoint concentration.

 This journal is © The Royal Society of Chemistry 2019

Published on 16 October 2019. Downloaded by University of Zurich on 1/3/2020 12:37:16 PM.

sensors were first functionalised with a hemagglutinin (HA) antibody prior to the conjugation of HA antigen-tagged anti-PD-1, anti-PD-L1, and anti-LAG-3 nanoyeast ScFvs (Fig. 1a). We selected biotin–avidin chemistry for HA antibody biosensor conjugation because this conjugation route provides a stable, dense, and strong modification that improves affinity probe orientation.[26,27] After a sample droplet was pipetted onto the biosensor (*i.e.*, 20 μL), the application of an ac-EHD field (V_{pp} = 800 mV, f = 500 Hz) resulted in *in situ* nanofluidic mixing in proximity to the biosensor surface (Fig. 1b). The ac-EHD nanofluidic mixing is engendered by the unequal accumulation of surface charges on the smaller ring and larger circular electrode that give rise to a body force moving the bulk liquid towards the larger electrode.[28] The flow stimulation increases the interactions of immune checkpoints with the nanoyeast ScFvs and also reduces non-specific biosensor binding. After sample incubation, the captured immune checkpoints are labelled with a HRP-conjugated secondary antibody (Fig. 1c). Subsequent addition of TMB solution results in a colour change mediated by the enzymatic oxidation of TMB in the presence of HRP from transparent to blue (maximal absorbance wavelength = 650 nm) or yellow (maximal absorbance wavelength = 450 nm) after reaction quenching with sulfuric acid. We selected the absorbance read-out at 450 nm because of its higher sensitivity and stability over the 650 nm read-out.[29]

3.2 MICB optimisation, specificity and sensitivity

Soluble PD-1, PD-L1, and LAG-3 are mainly released into circulation by their proteolytic cleavage from the cell membrane. The reported concentrations of these immune checkpoint molecules in circulation vary depending on disease types and stages.[30,31] Typically, sub-ng per mL concentrations have been reported. However, it was also commonly indicated that for prognostic applications lower detection limits are required. MICB was designed to enable sensitive detection of multiple immune checkpoints at sub-ng per mL concentrations. We opted to use *in situ* nanofluidic mixing, and robust and sensitive colorimetric reaction to improve assay sensitivity. To optimise the colorimetric read-out, we first investigated the time of TMB substrate incubation from 5 to 25 min. We found that the highest absorbance value using PD-1 standard spiked in buffer was at 20 min incubation (ESI Fig. S4†) and was used for further studies.

The stimulation of nanofluidic mixing promotes collisions of soluble immune checkpoints with the nanoyeast ScFv functionalised MICB and reaches a time-depending maximum. To investigate how the nanofluidic mixing time affects the detection sensitivity, we performed experiments using PD-1, PD-L1 and LAG-3 standards to study the incubation time from 10 to 75 min. Fig. 2a shows that the highest detection read-out was achieved at ≥40 min. 40 min target incubation under ac-EHD nanofluidic mixing was selected and compared with static target incubation (no ac-EHD field applied). As shown in Fig. 2b, the ac-EHD nanofluidic mixing increased the signal intensity by approx. 49 to 61% compared to static incubation. The increased signal intensity was a consequence of the improvement in mass transfer of soluble immune checkpoints to the sensor surface that was facilitated by ac-EHD nanofluidic mixing.

Liquid biopsy samples such as serum have a complex sample matrix that contains a high concentration of non-target molecules that can potentially interfere with the detection of low-abundant immune checkpoint markers. Ensuring adequate biosensor specificity is thus key for accurate and reliable target detection. To examine the specificity of the optimised MICB, the device was functionalised with target nanoyeast ScFvs. Samples containing target immune checkpoints (positive control), non-target immune checkpoints (negative control), and blank samples (negative control) were then analysed. A strong signal was obtained for the detection

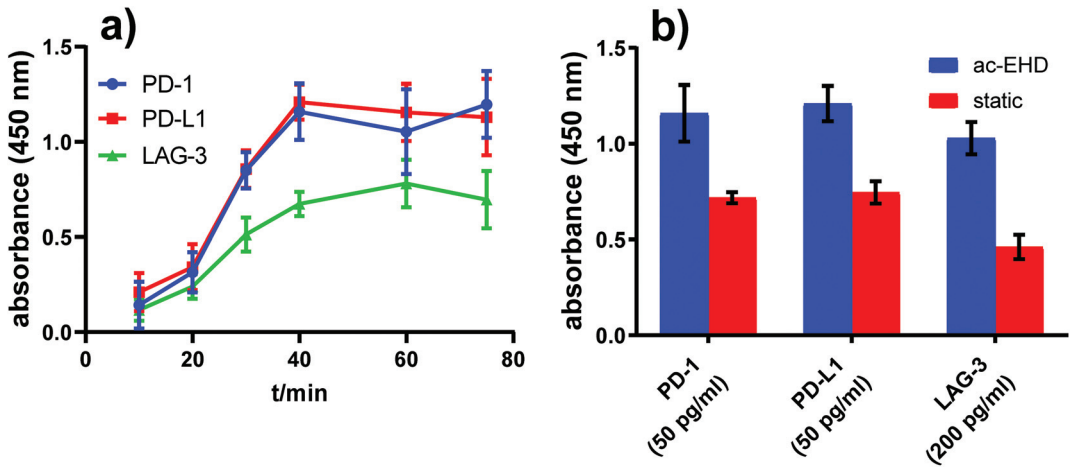

Fig. 2 (a) Effect of immune checkpoint incubation time under ac-EHD nanofluidic mixing on detection sensitivity. The analyte concentration was 50 pg mL^{-1} for PD-1 (blue), 50 pg mL^{-1} for PD-L1 (red), and 200 pg mL^{-1} for LAG-3 (green). (b) Comparison of detection sensitivity between the ac-EHD nanofluidic mixing MICB assay (blue) and the static assay (without ac-EHD, red). Error bars represent the standard deviation obtained from three replicate measurements.

Published on 16 October 2019. Downloaded by University of Zurich on 1/3/2020 12:37:16 PM.

of target immune checkpoints, while only a minimal non-specific signal resulted from the negative controls (Fig. 3, left panel). Similarly, the specificity of MICB functionalisation was probed by analysing target samples on an incompletely functionalised device devoid of nanoyeast ScFvs or HA antibody (negative controls) and only negligible signal intensities were observed for these experiments. In summary, MICB achieved reliable detection of PD-1, PD-L1, and LAG-3 through specific immune checkpoint capture using nanoyeast ScFvs.

To detect changes in circulating PD-1, PD-L1, and LAG-3 such as those that could occur during the immune checkpoint blockade therapy, the assay should provide a sufficient dynamic response. We investigated the sensitivity and dynamic response of MICB by analysing serially diluted

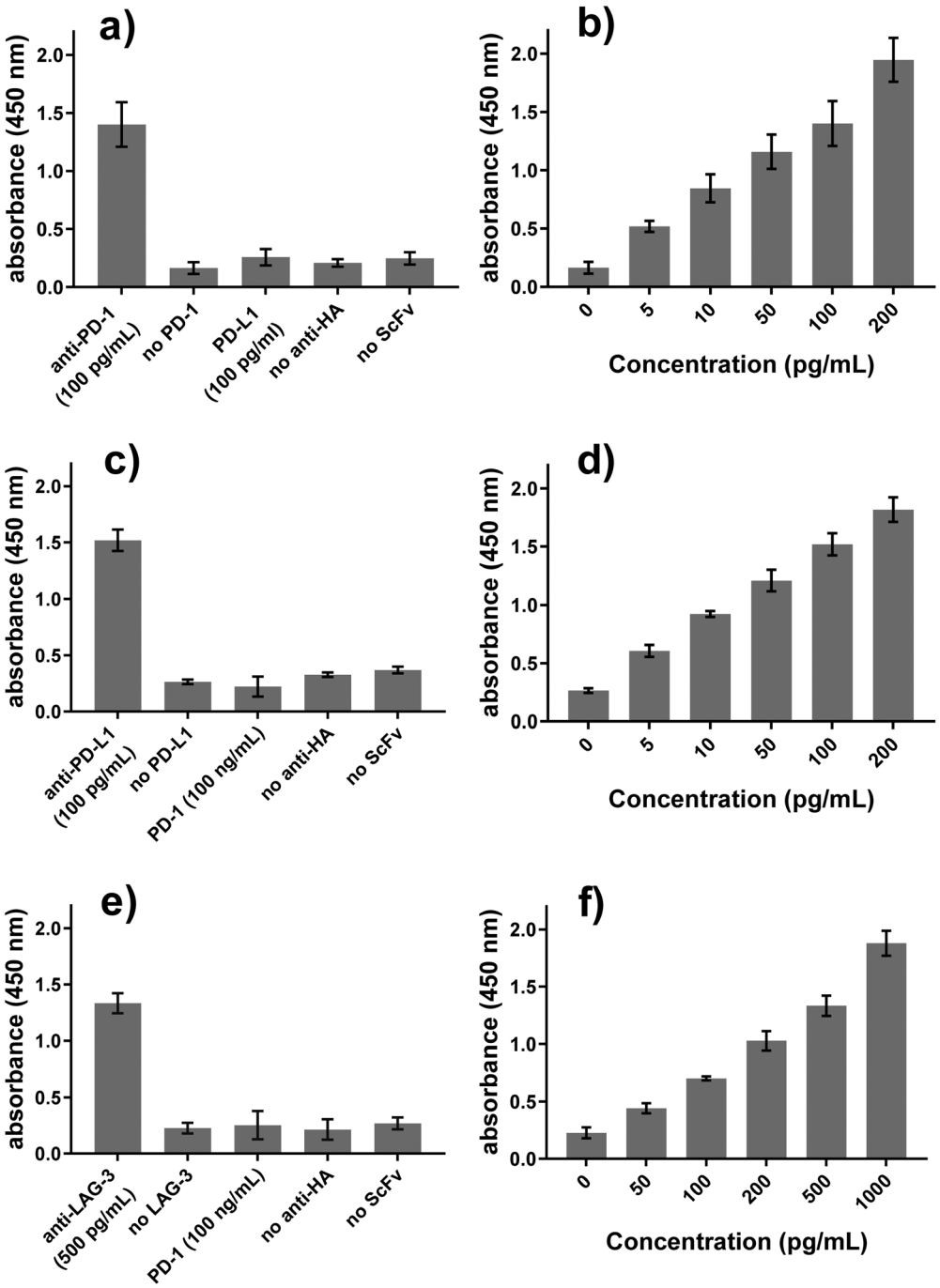

Fig. 3 Specificity and sensitivity of MICB. Absorbance signals obtained from the target detection of (a) PD-1, (c) PD-L1, and (e) LAG-3, and negative controls of the assay run without a target, with a non-target, and incomplete biosensor functionalisation devoid of an anti-HA antibody or nanoyeast ScFvs. Detection sensitivity obtained by serial dilution of the target in PBS for (b) PD-1, (d) PD-L1, and (f) LAG-3. Error bars show the standard deviation of three measurements.

 This journal is © The Royal Society of Chemistry 2019

Published on 16 October 2019. Downloaded by University of Zurich on 1/3/2020 12:37:16 PM.

samples with target concentrations of 0 to 1000 pg mL^{-1} (Fig. 3, right panel). MICB enabled accurate PD-1 and PD-L1 detection as low as 5 pg mL^{-1} with a dynamic response of 5 to 200 pg mL^{-1} and a coefficient of variation (CV) between 2.8 and 13.8%. For LAG-3, a gradual signal increase was observed from 50 to 1000 pg mL^{-1} with a CV of 2.5 to 11.4%. The LAG-3 detection limit was 50 pg mL^{-1}. These MICB analytical performance values enable the detection of soluble PD-1, PD-L1, and LAG-3 at prognostic concentrations in various cancers.[30]

3.3 MICB evaluation on stimulated liquid biopsy samples

To investigate the potential of MICB for the detection of soluble PD-1, PD-L1, and LAG-3 in liquid biopsy samples, we analysed simulated plasma samples that were fortified with target immune checkpoints at a prognostic cut-off concentration. The prognostic cut-off is defined as the threshold concentration of PD-1, PD-L1, and LAG-3 which could be used to make predictive statements about the patient's outcome. For instance, increased concentrations of soluble PD-1 and PD-L1 in patient plasma or serum were associated with decreased disease-free survival in various types of cancers.[30] The prognostic cut-off values for PD-1 in advanced rectal cancer and PD-L1 in lymphoma were set at 57 pg mL^{-1}.[32,33] For LAG-3, elevated levels of soluble LAG-3 in patients with gastric cancer, non-small-cell lung cancer, and estrogen or progesterone positive breast cancer were found to have improved disease-free and overall survival rates.[34–36] For breast cancer, the prognostic cut-off of LAG-3 in serum was set at 120 pg mL^{-1}.

We prepared stimulated liquid biopsy samples by spiking 50 pg mL^{-1} PD-1, 50 pg mL^{-1} PD-L1, and 120 pg mL^{-1} LAG-3 into diluted human serum. 20 μL of stimulated liquid biopsy sample was added to separate MICB sample wells. The MICB electrodes were individually functionalised with anti-PD-1, anti-PD-L1, or anti-LAG-3 nanoyeast ScFvs. Blank serum served as the negative control. After sample incubation under ac-EHD conditions of 800 mV and 500 Hz, the MICB assay was completed by incubations with the HRP-conjugated secondary antibody and TMB substrate solution. After 20 min, the substrate solution was withdrawn, quenched, and absorbance values were measured. The fortified serum samples provided a clearly differentiable signal response compared to the blank serum (Fig. 4) showing the potential of MICB for multiple immune checkpoint detection from small volumes of liquid biopsy samples.

Current gold standard methods for monitoring immune checkpoint markers are mostly based on mass spectrometry and ELISA. For example, Kruger *et al.* developed an ELISA method providing detection sensitivity as low as 10 pg mL^{-1} for PD-L1.[37] Zhang *et al.* developed a liquid chromatography and mass spectrometry based system to monitor different immune checkpoint markers. The method provided excellent sensitivity (0.07–1 ng mg^{-1} protein), accuracy (15.0% to 16.6% intra-batch accuracy) and multiplexing capability.[38] In comparison, our assay is relatively simple, applies a colorimetric read-out, and does not require expensive instrumentation. Moreover, MICB enables multiplex target analysis using a cost-effective antibody alternative (*i.e.* nanoyeast ScFv), and yet shows high sensitivity and specificity. We believe that monitoring of immune checkpoints might become increasingly important for example, for detecting early signs of non-responsiveness in patients undergoing immune checkpoint blockade therapy.[39] Furthermore, parallel detection of multiple immune checkpoint markers might support the study of immune checkpoint interactions and their potential synergistic effects.[1]

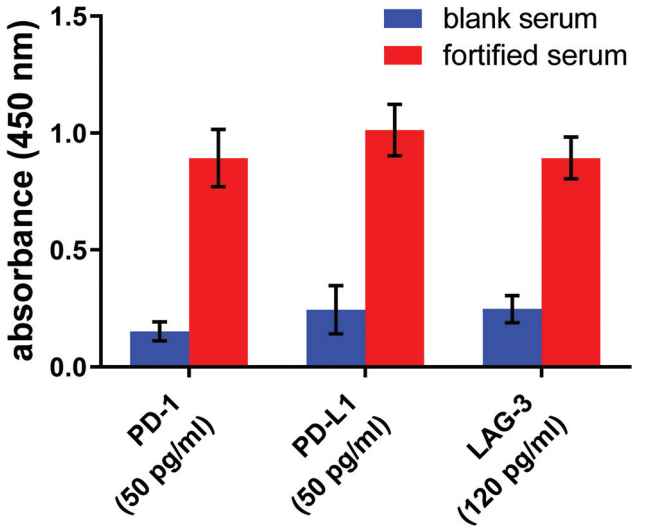

Fig. 4 Evaluation of MICB on simulated patient serum. PD-1, PD-L1, and LAG-3 were spiked into diluted human serum and analysed by using MICB (red). Blank serum samples served as the negative control (blue). Error bars represent the standard deviation of triplicate measurements.

4. Conclusion

We have demonstrated a multiplexed immune checkpoint biosensor (MICB) for parallel detection of PD-1, PD-L1, and LAG-3 in human serum. MICB incorporates nanofluidic mixing and nanoyeast ScFvs for specific target capture followed by a sensitive colorimetric read-out. Notably, MICB required only a single sample droplet per immune checkpoint, which is particularly attractive when only small sample volumes are available (*e.g.*, patient samples). Using MICB, the target immune checkpoints could be detected at concentrations as low as 5 pg mL^{-1} and up to 28 samples could be processed simultaneously in approx. 2 h supporting high-throughput and sensitive analysis. MICB also showed high potential for immune checkpoint detection at clinically-relevant concentrations in simulated patient serum, where the device's sensitivity met the prognostic cut-off concentrations of PD-1, PD-L1, and LAG-3 found in patient serum. We believe that the simplicity and capability for parallel analysis of MICB has the potential to detect a multitude of emerging immune checkpoint markers with promise to guide cancer immune therapy.

Conflicts of interest

There are no conflicts to declare.

Published on 16 October 2019. Downloaded by University of Zurich on 1/3/2020 12:37:16 PM.

Acknowledgements

This work was supported by the National Breast Cancer Foundation of Australia (CG-12-07), the UQ Development Fellowship (UQFEL1831057), and the University of Queensland ECR Grant (UQECR1945613). We also acknowledge funding from the Australian Research Council (DP160102836). These grants have significantly contributed to the environment to stimulate the research described here. Device fabrication was performed at the Australian National Fabrication Facility, Queensland node (ANFF-Q).

References

1 D. M. Pardoll, *Nat. Rev. Cancer*, 2012, **12**, 252–264.
2 S. Sau, H. O. Alsaab, K. Tatiparti, K. Bhise, A. K. Iyer, R. Alzhrani and S. K. Kashaw, *Front. Pharmacol.*, 2017, **8**, 1–15.
3 L. P. Andrews, A. E. Marciscano, C. G. Drake and D. A. A. Vignali, *Immunol. Rev.*, 2017, **276**, 80–96.
4 H. Meng and M. C. Fitzgerald, *J. Proteome Res.*, 2018, **17**, 1129–1137.
5 Y. He, C. J. Rivard, L. Rozeboom, H. Yu, K. Ellison, A. Kowalewski, C. Zhou and F. R. Hirsch, *Cancer Sci.*, 2016, **107**, 1193–1197.
6 K. Takahashi, M. Ohira, Y. Asano, T. Morisaki, K. Takada, T. Takashima, S. Kashiwagi, W. Goto, K. Hirakawa, M. Ohsawa, S. Tomita and H. Fujita, *J. Transl. Med.*, 2018, **16**, 1–12.
7 H. Xiao, B. Huang, Y. Yuan, D. Li, L. F. Han, Y. Liu, W. Gong, F. H. Wu, G. M. Zhang and Z. H. Feng, *Clin. Cancer Res.*, 2007, **13**, 1823–1830.
8 D. Gu, X. Ao, Y. Yang, Z. Chen and X. Xu, *J. Immunother. Cancer*, 2018, **6**, 1–14.
9 Y. S. Grewal, M. J. A. Shiddiky, S. M. Mahler, G. A. Cangelosi and M. Trau, *ACS Appl. Mater. Interfaces*, 2016, **8**, 30649–30664.
10 K. K. Reza, A. A. I. Sina, A. Wuethrich, Y. S. Grewal, C. B. Howard, D. Korbie and M. Trau, *Biosens. Bioelectron.*, 2018, **126**, 178–186.
11 Y. Wang, S. Rauf, Y. S. Grewal, L. J. Spadafora, M. J. A. Shiddiky, G. A. Cangelosi, S. Schlücker and M. Trau, *Anal. Chem.*, 2014, **86**, 9930–9938.
12 S. R. Doonan, M. Lin and R. C. Bailey, *Lab Chip*, 2019, **19**, 1589–1598.
13 S. T. Sanjay, G. Fu, M. Dou, F. Xu, R. Liu, H. Qi and X. Li, *Analyst*, 2015, **140**, 7062–7081.
14 A. Wuethrich and J. P. Quirino, *Anal. Chim. Acta*, 2019, **1045**, 42–66.
15 M. Sonker, E. K. Parker, A. V. Nielsen, V. Sahore and A. T. Woolley, *Analyst*, 2018, **143**, 224–231.
16 M. J. Beauchamp, A. V. Nielsen, H. Gong, G. P. Nordin and A. T. Woolley, *Anal. Chem.*, 2019, **91**, 7418–7425.
17 M. Sonker, V. Sahore and A. T. Woolley, *Anal. Chim. Acta*, 2017, **986**, 1–11.
18 S. Dey, K. Koo, Z. Wang, A. A. I. Sina, A. Wuethrich and M. Trau, *Lab Chip*, 2019, **19**, 738–748.
19 K. R. Khondakar, S. Dey, A. Wuethrich, A. A. I. Sina and M. Trau, *Acc. Chem. Res.*, 2019, **52**, 2113–2123.
20 J. Li, J. Wang, Y. S. Grewal, C. B. Howard, L. J. Raftery, S. Mahler, Y. Wang and M. Trau, *Anal. Chem.*, 2018, **90**, 10377–10384.
21 A. Wuethrich, C. B. Howard and M. Trau, *Microchem. J.*, 2018, **137**, 231–237.
22 A. Wuethrich, A. A. I. Sina, M. Ahmed, T.-Y. Lina, L. G. Carrascosa and M. Trau, *Nanoscale*, 2018, **10**, 10884–10890.
23 R. Fan, O. Vermesh, A. Srivastava, B. K. H. Yen, L. Qin, H. Ahmad, G. A. Kwong, C. C. Liu, J. Gould, L. Hood and J. R. Heath, *Nat. Biotechnol.*, 2008, **26**, 1373–1378.
24 H. Chen, C. Chen, S. Bai, Y. Gao, G. Metcalfe, W. Cheng and Y. Zhu, *Nanoscale*, 2018, **10**, 20196–20206.
25 A. A. I. Sina, M. T. Foster, D. Korbie, L. G. Carrascosa, M. J. A. Shiddiky, J. Gao, S. Dey and M. Trau, *Analyst*, 2017, **142**, 3573–3578.
26 S. Avvakumova, M. Colombo, P. Tortora and D. Prosperi, *Trends Biotechnol.*, 2014, **32**, 11–20.
27 P. M. Wolny, J. P. Spatz and R. P. Richter, *Langmuir*, 2010, **26**, 1029–1034.
28 A. Ramos, A. González, A. Castellanos, N. G. Green and H. Morgan, *Phys. Rev. E: Stat., Nonlinear, Soft Matter Phys.*, 2003, **67**, 056302.
29 A. Frey, B. Meckelein, D. Externest and M. A. Schmidt, *J. Immunol. Methods*, 2000, **233**, 47–56.
30 X. Zhu and J. Lang, *Oncotarget*, 2017, **8**, 97671–97682.
31 L. Long, X. Zhang, F. Chen, Q. Pan and P. Phiphatwatchara, *Genes Cancer*, 2018, **9**, 176–189.
32 D. Rossille, M. Gressier, D. Damotte, D. Maucort-Boulch, C. Pangault, G. Semana, S. Le Gouill, C. Haioun, K. Tarte, T. Lamy, N. Milpied, T. Fest, G. Damaj, A. Clavert, A. Al Jijakli, A. Banos, J. L. Dutel, E. Deconinck, P. Rodon, K. Bouabdallah, P. Soubeyran, B. Choufi, A. Maakaroun, O. Tournilhac, J. Fleury, R. Gressin, H. Maisonneuve, K. Laribi, P. Solal-Celigny, P. Moreau, J. F. Rossi, G. Cartron, N. Morineau, J. L. Harousseau, E. Jourdan, M. Alexis, F. Dreyfus, V. Delwail, J. Cornillon, R. Garidi, E. Gyan, P. Colombat and P. Godemer, *Leukemia*, 2014, **28**, 2367–2375.
33 T. Tominaga, T. Akiyoshi, N. Yamamoto, S. Taguchi, S. Mori, T. Nagasaki, Y. Fukunaga and M. Ueno, *PLoS One*, 2019, **14**, 1–11.
34 N. Li, B. Jilisihan, W. Wang, Y. Tang and S. Keyoumu, *Cancer Biomarkers*, 2018, **23**, 341–351.
35 Y. He, C. Zhou and F. R. Hirsch, *OncoTargets Ther.*, 2018, **11**, 4781–4784.
36 F. Triebel, K. Hacene and M. F. Pichon, *Cancer Lett.*, 2006, **235**, 147–153.

 This journal is © The Royal Society of Chemistry 2019

37 S. Kruger, M. L. Legenstein, V. Rösgen, M. Haas, D. P. Modest, C. B. Westphalen, S. Ormanns, T. Kirchner, V. Heinemann, S. Holdenrieder and S. Boeck, *OncoImmunology*, 2017, **6**, 1–8.
38 Q. Zhang, R. Salzler, A. Dore, J. Yang, D. Ma, W. C. Olson and Y. Liu, *J. Proteome Res.*, 2018, **17**, 3932–3940.
39 N. L. Syn, M. W. L. Teng, T. S. K. Mok and R. A. Soo, *Lancet Oncol.*, 2017, **18**, e731–e741.

Published on 16 October 2019. Downloaded by University of Zurich on 1/3/2020 12:37:16 PM.